Temperature dependent XAFS studies of local atomic structure of the perovskite-type zirconates

V. Vedrinskii, E. Nazarenko, M. Lemeshko, V. Nassif, O. Proux, A. Novakovich, Y. Joly

Temperature dependent XAFS studies of local atomic structure of the perovskite-type zirconates

R. V. Vedrinskii,[1] E. S. Nazarenko,[1,2] M. P. Lemeshko,[1] V. Nassif,[3,5] O. Proux,[4,5] A. A. Novakovich,[1] and Y. Joly[2]
[1]*Institute of Physics, Rostov State University, 194 Stachky Avenue, Rostov-on-Don 344090, Russia*
[2]*Laboratoire de Cristallographie, CNRS, l'Université Joseph Fourier, 166 Boîte Postale, F-38042 Grenoble Cedex 9, France*
[3]*CEA/Grenoble, DRFMC/SP2M/NRS, F-38054 Grenoble Cedex 9, France*
[4]*Laboratoire de Géophysique Interne et Tectonophysique, UMR CNRS, Université Joseph Fourier, F-38400 Saint-Martin-D'Hères, France*
[5]*BM30b CRG-FAME, European Synchrotron Radiation Facility, F-38043 Grenoble Cedex 9, France*
(Received 31 July 2005; revised manuscript received 8 March 2006; published 17 April 2006)

Temperature dependent preedge and extended x-ray absorption fine structure measurements at the Zr *K* edge for the perovskite-type zirconates $PbZr_{0.515}Ti_{0.485}O_3$ (PZT), $PbZrO_3$ (PZ), and $BaZrO_3$ are performed. To carry out a more accurate study of the weak reconstruction of the local atomic structure we employed a combination of two techniques: (i) analysis of the preedge fine structure, and (ii) analysis of the Fourier transform of the difference between $\chi(k)$ functions obtained at different temperatures. A detailed investigation of local atomic structure in the cubic phase for all the crystals is also performed. It is shown that neither the displacive nor the order-disorder model can describe correctly the changes of local atomic structure during phase transitions in PZ and PZT. A spherical model describing the local atomic structure of perovskite-type crystals suffering structural phase transitions is proposed.

DOI: 10.1103/PhysRevB.73.134109 PACS number(s): 61.10.Ht, 63.90.+t, 77.90.+k

I. INTRODUCTION

Perovskite-type materials are fundamentally and technologically important for their ferroelectric and piezoelectric properties. Most of the perovskite oxides are cubic at high temperatures and often have a variety of lower-symmetry phases at lower temperatures. To realize the microscopic nature of the phase transitions in perovskites, it is important to ascertain how their local atomic structure changes as a function of temperature especially near the phase transition points. Nowadays the most widespread methods of local structure studies employ x-ray absorption fine structure (XAFS). In this contribution we investigate the temperature dependence of the local atomic structure for perovskite-type zirconates using XAFS of Zr *K* spectra in both the extended (EXAFS) and preedge regions.

Among the materials under consideration the ferroelectric $PbZr_{1-x}Ti_xO_3$ solid solutions have attracted special attention owing to their unusually large piezoelectric coefficients near the morphotropic phase boundary which divides regions with tetragonal and rhombohedral structures.[1] This fact allows using the $PbZr_{1-x}Ti_xO_3$ ceramics in various piezoelectric and ferroelectric devices. The results obtained in this paper for $PbZr_{0.515}Ti_{0.485}O_3$ (PZT) are compared with those obtained for lead zirconate $PbZrO_3$ (PZ), which is an end member of the PZT solid solutions, and crysalline paraelectic $BaZrO_3$ (BZ), which is cubic at all temperatures.

The local structure rearrangement during phase transitions in perovskite-type crystals is under discussion for several decades. Nowadays two alternative structural models are often used for perovskite-type materials. The first, "displacive" model[2] assumes that in the low-temperature phases cation sites are displaced along the polar axes relative to the oxygen framework and in the cubic phase they are located in the ideal perovskite positions. According to another, the so-called "eight-site" model,[3] the cations are displaced from the centers of oxygen octahedrons to off-center positions located along eight ⟨111⟩ directions in all the phases. The number of such off-center positions occupied by the cations changes as a result of phase transitions, which are considered to be of the order-disorder type. The eight-site model is not a unique *n*-site model to describe the phase transitions in perovskites. In particular, six- and 12-site models can also be used.[4] According to them the cations are displaced from the centers of oxygen octahedrons along the axes of fourfold and twofold symmetry, respectively.

The results of EXAFS studies of perovskite-type oxides are contradictory. Some authors did not find significant change of the first-shell contribution to EXAFS at the phase transition points for the powder samples and hence considered the eight-site model to be valid[5,6] and the transitions to be of the order-disorder type. However, analysis of the polarized XAFS performed for single crystals showed that in the low-temperature phases the displacive model is in good agreement with the experimental data, whereas the eight-site model provides better agreement with the local atomic structure in the cubic phase.[7,8] The idea that different models of local atomic structure are appropriate in different phases was recently supported by first-principles calculations[9] and NMR studies[10] of the atomic structure of the $BaTiO_3$ crystal.

In the present paper the XAFS of Zr *K* spectra obtained for powder samples is employed. To carry out a more accurate study of local atomic structure reconstruction, a combination of two methods is used: (i) differential analysis of the preedge fine structure (PEFS), and (ii) the "differential EXAFS" method, i.e., the analysis of the Fourier transform of the difference between $\chi(k)$ functions obtained for different temperatures.

II. EXPERIMENT

Powder samples of $BaZrO_3$ and $PbZr_{0.515}Ti_{0.485}O_3$ were prepared at the Institute of Physics at Rostov State Univer-

sity by standard solid-state reactions of $BaCO_3$, ZrO_2 and PbO, ZrO_2, TiO_2, respectively. Several grindings and firings in air at temperatures up to 1300 °C for BZ and 1240 °C for PZT were performed. To prepare the PZ sample a single crystal was milled. X-ray powder diffraction measurements confirmed that the samples were single-phase ones.

Preedge and EXAFS Zr *K*-edge spectra were collected at the European Synchrotron Radiation Facility (ESRF, Grenoble, France) at the beamline BM30b (FAME).[11] The storage ring was run at energy 6.0 GeV with the electron current about 30 mA. Spectra were recorded in the transmission mode using a double-crystal Si(220) monochromator. The full fan delivered by the bending magnet source was focused in the horizontal plane by the second crystal of the monochromator and by the second Rh-coated mirror in the vertical plane. Harmonic rejection is achieved with two Rh-coated mirrors, before and after the monochromator. Finally, a feedback system was used to maximize the output of the two-crystal x-ray monochromator. The spectra were scanned in the range of 17.8–19.22 keV, with a 0.5 eV energy step. The samples were prepared from ground ceramic diluted with BN and pressed into tablets.

K-edge x-ray absorption spectra for PZT ceramics were measured at room temperature, which is the lowest temperature of the tetragonal phase,[1] at the temperature 100 °C, which is far from any phase transition, at 300 °C, which is close to the Curie point (360 °C), and at 500 °C in the paraelectric cubic phase. For comparison purposes the spectra for PZ and BZ were collected for the same set of temperatures. At 20 and 100 °C the PZ crystal is monoclinic with antiferroelectric displacements of Zr atoms. The Curie temperature for PZ is about 230 °C.[12,13] Thus for the spectra measurements at 300 and 500 °C PZ was in the cubic phase far from the phase transition point. BZ is cubic for all the temperatures.[14]

III. RESULTS AND DISCUSSION

A. Preedge fine structure analysis

The preedge fine structure of the *B* atom *K* absorption spectrum provides valuable information on the local atomic structure of BO_6 octahedrons in ABO_3 perovskite crystals. PEFS appears before the main rise of the *B K* spectrum and it is caused by transitions of the *B* atom 1s electrons to the lower conduction bands originating from atomic *d* states of the transition metal atoms *B*. As was shown earlier,[15] if the *B* atoms are displaced from their centrosymmetrical positions, in the *B* atom PEFS there appears an additional peak, which is absent otherwise. This peak is caused by mixing of unoccupied *p* and *d* states of the *B* atom and it is called "the *p-d* peak" hereafter. As was shown by calculations,[15] the *p-d* peak is significantly more sensitive to local distortions of the BO_6 octahedrons than other features of the PEFS. For a polycrystalline sample the total area *I* under this peak is proportional to the mean-square displacement (MSD) $\langle(\Delta\vec{x})^2\rangle$ of the *B* atom from the center of the BO_6 octahedron:[15]

$$I \sim \sum_i \langle(\Delta x_i)^2\rangle = \langle(\Delta\vec{x})^2\rangle, \tag{1}$$

where Δx_i is the displacement of the *B* atom from the center of the *i*th O-*B*-O atomic chain ($i=1,2,3$) along this chain and $\langle(\Delta x_i)^2\rangle$ is the corresponding MSD. If the x-ray electric field vector $\vec{e}$ is directed along the *i*th O-*B*-O chain of a single-crystal sample, the *p-d* peak area is proportional to $\langle(\Delta x_i)^2\rangle$.

Experimental studies of the Ti *K* x-ray absorption near-edge structure (XANES) for a $PbTiO_3$ (PT) single crystal[16] have shown strong angular and temperature dependence of the *p-d* peak. It was found that if $\vec{e}$ is parallel to the axis of fourfold symmetry of the tetragonal PT crystal this peak is very intense at room temperature and decreases when the temperature increases. On the contrary, if $\vec{e}$ is perpendicular to this axis the *p-d* peak is weak at room temperature and it increases at higher temperatures. In agreement with the calculations, other features of the PEFS are nearly independent of temperature and polarization. At the same time, the averaged *p-d* peak area determined from the Ti *K* spectrum of a powder PT sample[17] slightly decreases when the temperature increases. This result seems to be quite strange since, according to (1), the averaged *p-d* peak area is proportional to the MSD of the Ti atom from the center of the TiO_6 octahedron and one can expect that this value should increase at higher temperatures. Such an expected dependence of the *p-d* peak area on temperature really takes place for the $EuTiO_3$ crystal, which is paraelectric at all temperatures and does not suffer structural phase transitions[18] unlike the ferroelectric PT crystal.

The results obtained for the niobates $KNbO_3$ (KN) and $NaNbO_3$ (NN), which undergo structural phase transitions, are similar to those for PT. The Nb *K* XAFS studies performed for KN (Refs. 7 and 8) and NN (Ref. 19) single crystals showed strong dependence of the preedge area on temperature and polarization. On the other hand the averaged preedge area determined from the Nb *K* spectra measured for the powder samples is almost temperature independent in a wide temperature interval.

These results can be reasonably explained within the following assumption. The potential surface for the atom *B* can be approximated by one of the three curves shown in Fig. 1, where *r* is the distance from the atom *B* to the immediate center of the BO_6 octahedron. In the case of paraelectric ABO_3 crystals with harmonic crystal lattice dynamics ($EuTiO_3$) the potential surface is a parabolic function shown by curve Fig. 1(a) (one-site model) (single-well potential surface). In such a case the MSD and the averaged preedge area increase, when the temperature increases, in agreement with the experiment. In the case of anharmonic ABO_3 crystals suffering structural phase transitions (PT, KN, and NN) the most probable potential surfaces take on the deep-double-well [Fig. 1(b)] and shallow-double well [Fig. 1(c)] forms. The maximum value of the deep-double-well potential curve in Fig. 1(b) ($r=0$) very much exceeds the minimum one ($r=r_0$). This means that the difference between these two values is much greater than the temperature measured in the energy scale. In such a case the MSD and the averaged preedge area are almost temperature independent as they really are in the case of KN and NN. On the contrary, the maximum value of the shallow-double-well potential curve [Fig. 1(c)] slightly exceeds the minimum one. Then the MSD and the averaged preedge area decrease when the tempera-

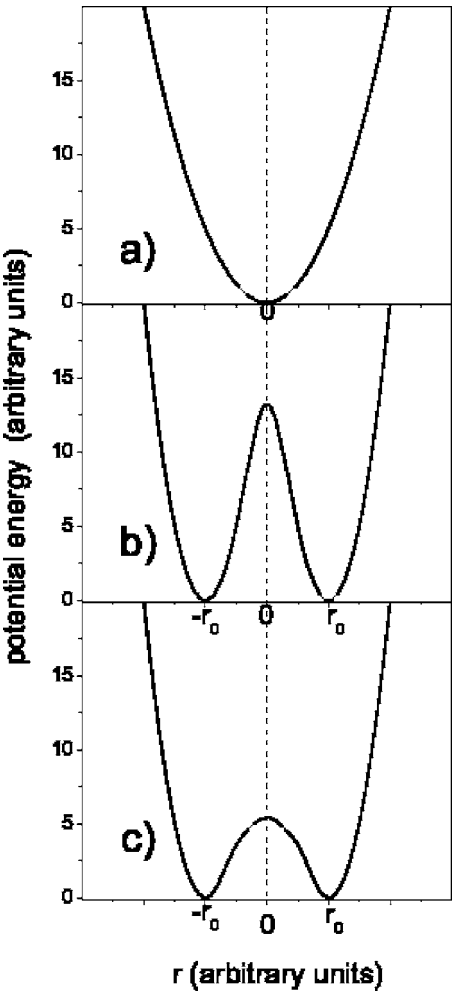

FIG. 1. The potential surfaces for the atom B in different ABO_3 perovskites: (a) $EuTiO_3$ and $BaZrO_3$, (b) $KNbO_3$, $PbZrO_3$, $PbZr_{0.515}Ti_{0.485}O_3$, and (c) $PbTiO_3$, r is the distance from the atom B to the center of the BO_6 octahedron.

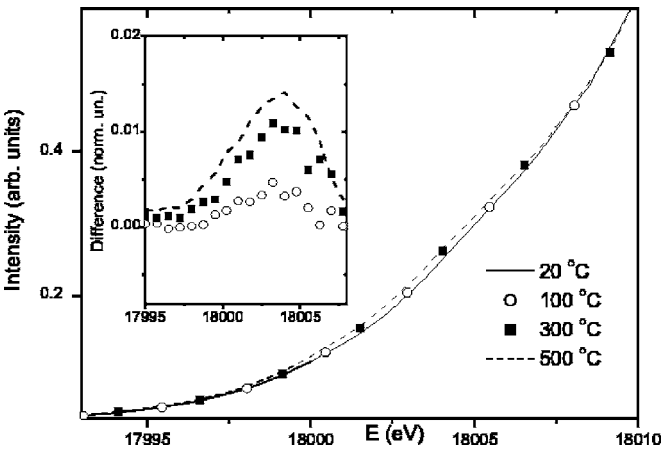

FIG. 2. Preedge region of the Zr K spectrum at different temperatures for $BaZrO_3$. Inset: difference between the spectra for 100, 300, and 500 °C and that for 20 °C.

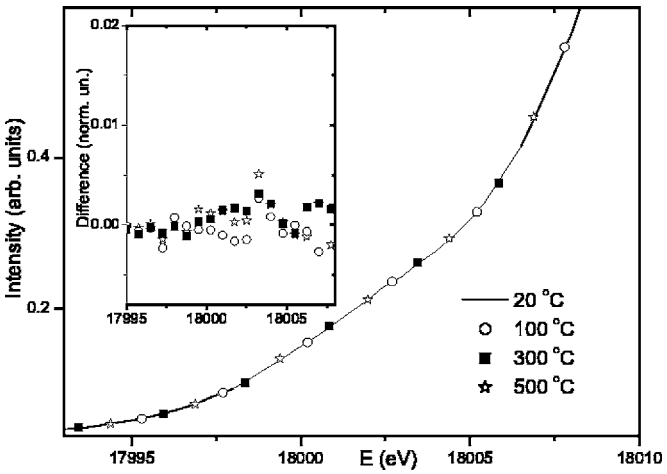

FIG. 3. Preedge region of the Zr K spectrum at different temperatures for $PbZrO_3$. Inset: difference between the spectra for 100, 300, and 500 °C and that for 20 °C.

ture increases as is the case of PT. Certainly, the potential surfaces under consideration are angularly dependent, but the preedge structure measurements performed for powder samples do not provide information on this dependence.

The preedge regions of the experimental Zr K XANES spectra for BZ, PZ, and PZT powder samples obtained in the present investigation are shown in Figs. 2–4. The differences between the spectra measured at higher temperatures and at the room temperature are presented in the insets. Unfortunately, it is impossible to analyze the PEFS of the Zr K spectra in more detail, as is possible in the case of PT, due to the large Zr K hole width ($\gamma_K \approx 3.84$ eV) but taking into account the results for PT mentioned above,[16] one can reasonably assume that the dependence of the total preedge area on temperature is mainly caused by the p-d peak. In order to study the sensitivity of the total preedge area to the MSD $\langle(\Delta\vec{x})^2\rangle$, the Zr K XANES spectra for the cubic BZ crystal were calculated for different displacements of the Zr atom from its centrosymmetrical position in the cubic lattice. The simulations were performed by the full multiple scattering

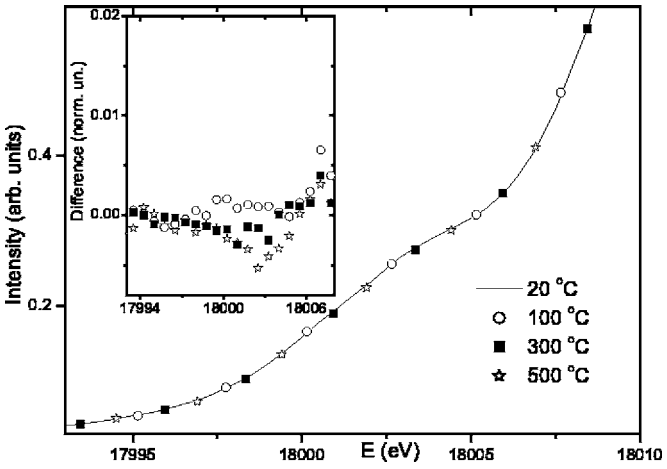

FIG. 4. Preedge region of the Zr K spectrum at different temperatures for $PbZr_{0.515}Ti_{0.485}O_3$. Inset: difference between the spectra for 100, 300, and 500 °C and that for 20 °C.

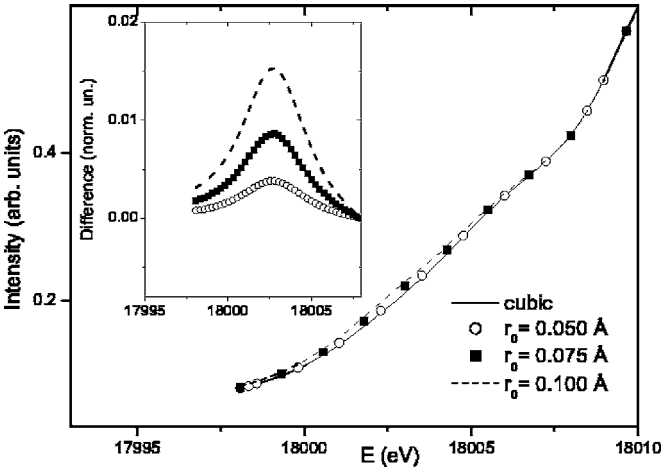

FIG. 5. The results of PEFS calculations for $BaZrO_3$ performed for different displacements r_0 of the Zr atom from its centrosymmetrical position in the cubic lattice. Inset: difference between the spectra calculated for different Zr atom displacements and that for ideal perovskite lattice.

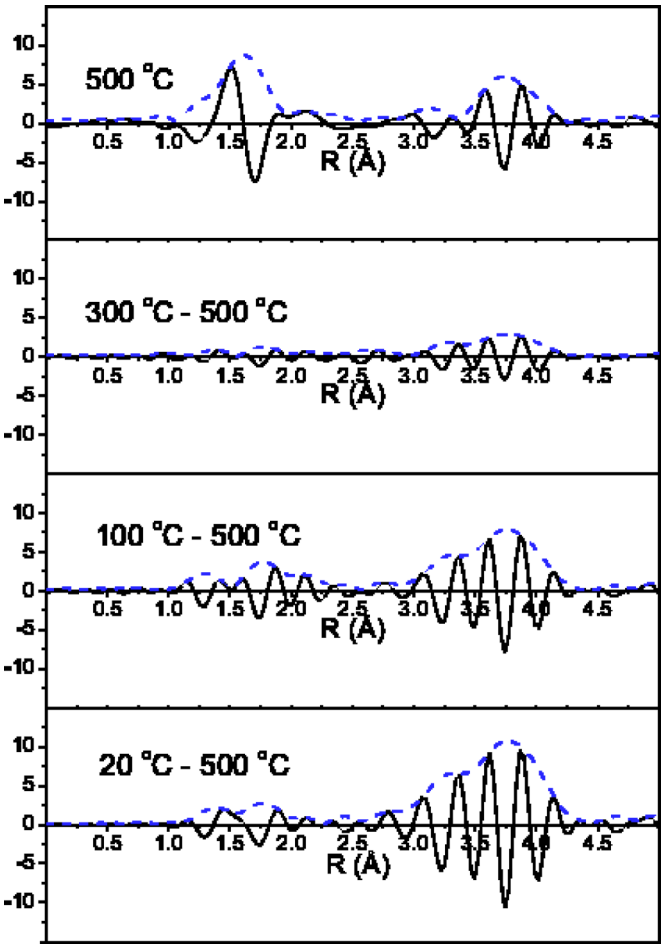

FIG. 6. (Color online) Absolute values [dashed (blue) lines] and real parts [solid (black) lines] of the k^3 weighted FT of the Zr EXAFS signal measured at 500 °C (on the top) and the differential FT for $BaZrO_3$. The temperatures are indicated in the figure.

TABLE I. Parameters of the first coordination shell for the $BaZrO_3$ crystal at different temperatures. N, coordination number, R, Zr–O distance, and σ^2, Debye-Waller factor.

T (°C)	N	R (Å)	σ^2 (Å^2)	R factor (%)
20	6	2.11	0.0020	0.7
100	6	2.11	0.0022	1.5
300	6	2.12	0.0039	1.2
500	6	2.12	0.0047	1.6

method using the XKDQ code.[15,20] The calculated spectra were broadened taking into account the Zr K hole width and experimental resolution. The results obtained are presented in Fig. 5. One can see in the inset that the differences between the spectra calculated for different Zr atom displacements and those experimentally obtained for BZ (Fig. 2) are of the same order. On the contrary, the analogous variations of the PEFS experimentally obtained for PZ and PZT crystals are significantly less. These results reveal that the potential surface for the Zr atom in the BZ crystal is similar to a single well, whereas PZ and PZT can be described within the deep-double-well model.

Using PEFS data we estimated also the average displacements $r_0=\sqrt{\langle(\Delta\vec{x})^2\rangle}$ of the B atoms from the centers of the BO_6 octahedrons. Comparing Figs. 3–5 one can conclude that the r_0 value for PZ is essentially less than that for PZT and does not exceed 0.1 Å. This estimation is in agreement with the diffraction data for PZ at room temperature, which gives $r_0 \approx 0.075$ Å within the assumption that local and global structures are close to each other at room temperature as they are for the KN crystal.[7,8]

Taking into account the results presented above, one can conclude that the PEFS data for the perovskite-type oxides suffering structural phase transitions, such as KN, NN, PZ, and PZT, make plausible a spherical model of their local atomic structure. According to this model, an atom B (Nb, Zr, Ti) is situated near the surface of a sphere of small radius r_0 ("central" sphere) at all temperatures. The center of this sphere coincides with the immediate center of the BO_6 octahedron at each moment. The distribution of the B atom on the surface of the central sphere can be complicated and can change significantly with temperature. The last statement is supported by the results of the PEFS studies performed for KN and NN single crystals.[7,8,19] The spherical model is a generalization of the n-site models that are often considered.[3,4] It is supposed in the n-site models that on the surface of the central sphere there are several sites, whose positions, contrary to the spherical model, do not vary depending on temperature and only their occupancies are temperature dependent. The spherical model, like the n-site models, is obviously inconsistent with the displacive model of phase transitions in the perovskites. The spherical model also does not presume the order-disorder model of the phase transitions, since these transitions, according to the spherical model, can result in complicated redistribution of the B atoms on the surface of the central sphere.

B. EXAFS Analysis

The local atomic structure of the ZrO_6 octahedrons for BZ, PZ, and PZT was also studied by a Zr K-edge EXAFS

TABLE II. Parameters of the first coordination shell for $PbZrO_3$ and $PbZr_{0.515}Ti_{0.485}O_3$ in the cubic phase (500 °C). N, coordination number, R, Zr-O distance, r_0, radius of the central sphere, σ^2, Debye-Waller factor, R_0, average Zr-O distance determined from the full first shell PRDF, and Σ^2, variance of the PRDF.

Model	N	R (Å)	r_0 (Å)	σ^2 (Å^2)	R_0 (Å)	Σ^2 (Å^2)	R factor (%)	$R\nu$ factor (%)
				$PbZrO_3$				
One site	6	2.11	0	0.0070	2.11	0.0070	1.9	0.3
Eight site	3	2.07	0.075	0.0050	2.11	0.0069	1.7	0.27
	3	2.15	0.075	0.0050				
Twelve site	2	2.06	0.075	0.0035	2.11	0.0067	1.7	0.32
	2	2.11	0.075	0.0076				
	2	2.16	0.075	0.0035				
				$PbZr_{0.515}Ti_{0.485}O_3$				
One site	6	2.09	0	0.0070	2.09	0.0067	3.5	0.44
Eight site	3	2.05	0.1	0.0024	2.11	0.0077	0.8	0.1
	3	2.17	0.1	0.0063				
Twelve site	2	2.04	0.1	0.0019	2.11	0.0079	0.9	0.13
	2	2.11	0.1	0.0040				
	2	2.18	0.1	0.0077				

analysis. The EXAFS processing was performed by the IFEFFIT package.[21] The selection of the best set of variables for each model follows from the minimum value of the figure-of-merit criterion in this program, denoted the R factor.[22] Scattering paths were determined by the FEFF7 code.[23]

We performed a complete analysis for the first coordination shell of the Zr atom for the cubic BZ crystal at all temperatures and for PZ and PZT in the cubic phase at 500 °C. Owing to the low symmetry of PZ and PZT at lower temperatures, the EXAFS fitting is unreliable in this case due to the great number of structural parameters to be determined. To investigate the reconstruction of the pair radial distribution function (PRDF) for PZ and PZT at lower temperatures we employed the Fourier transforms (FTs) of the difference normalized EXAFS functions $\chi_T(k)-\chi_{500}(k)$,

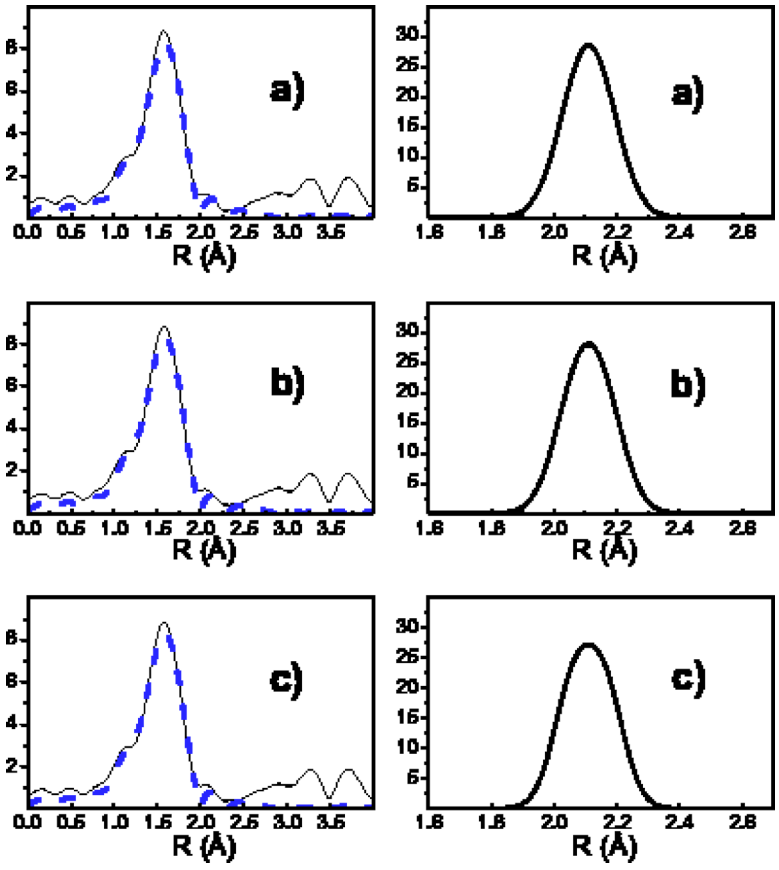

FIG. 7. (Color online) The results of fitting performed for different structural models for $PbZrO_3$: (a) one-, (b) eight-, and (c) 12-site model. Left panels: absolute values of the Fourier transform of the k^3 weighted $\chi(k)$ [solid (black) lines, experiment; dashed (blue) lines, fitting results]. Right panels: pair radial distribution functions.

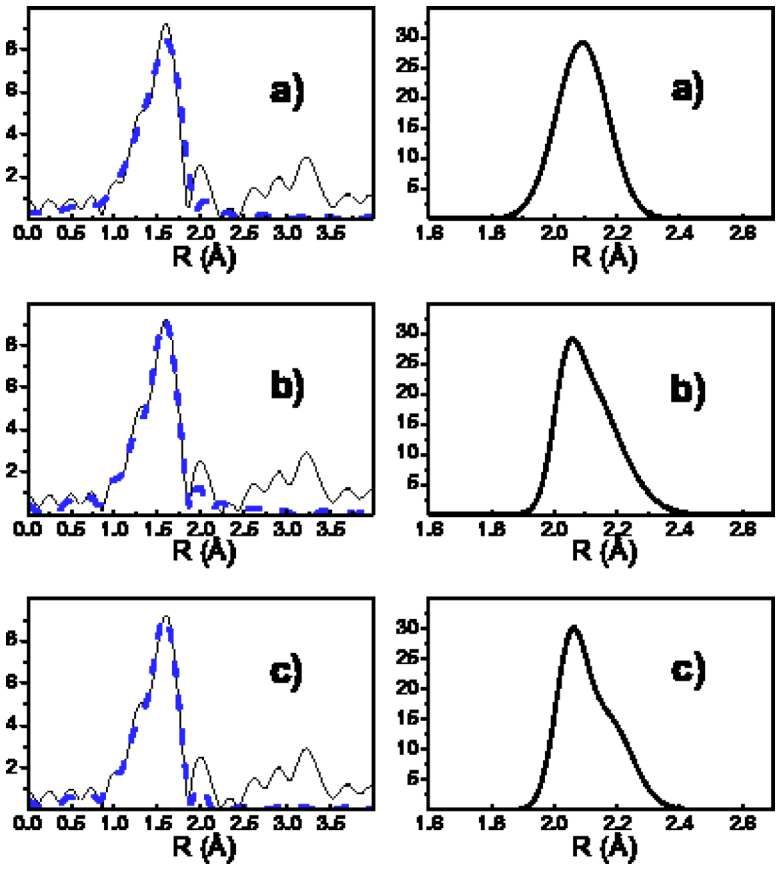

FIG. 8. (Color online) The results of fitting performed for different structural models for $PbZr_{0.515}Ti_{0.485}O_3$: (a) one-, (b) eight-, and (c) 12-positional model. Left panels: absolute values of the Fourier transform of the k^3 weighted $\chi(k)$ [solid (black) lines, experiment; dashed (blue) lines, fitting results]. Right panels: pair radial distribution functions.

where $\chi_{500}(k)$ is the signal obtained at 500 °C and $\chi_T(k)$ is that measured at the temperature T.

The Fourier transforms of the difference-normalized EXAFS functions for BZ are shown in Fig. 6. One can see that the variations of the first coordination shell signal are relatively small and the main feature of the difference FT for BZ is a modification of the third coordination shell signal [in the R range 3.8–4.2 Å which corresponds to the third (Zr) shell]. Most probably this is caused by an increase of the magnitude of the "tilting" mode vibrations on temperature. Such an effect destroys the linear Zr–O–Zr atomic chains and, as a result, demolishes the focusing processes in these chains and causes a decrease of the third coordination shell signal.

The BZ spectrum was analyzed within the one-site model for all temperatures. The k range for the Fourier transformation was 2.8–11.2 $Å^{-1}$. Fitting was performed in the R range 0.9–1.9 Å. The results are presented in Table I. One can see that the PRDF is a Gaussian with high accuracy at all the temperatures. Hence, both EXAFS and PEFS data prove the lattice dynamics of the $BaZrO_3$ crystal to be harmonic in the temperature range considered. This conclusion is in agreement with the absence of phase transitions for BZ.

The EXAFS data processing for PZ and PZT at 500 °C was performed for different models of their local atomic structure: one-, eight-, 12-, and six-site models and the uniform model. According to the last one, the Zr atom is uniformly distributed on the surface of the central sphere. In that case it was possible to synthesize the analytical PRDF and then to calculate the XAFS function with the radius of the central sphere and the Debye-Waller factor as parameters. At the same time for the n-site models the standard fitting with the IFEFFIT code was performed. The k range for the Fourier transformation was reduced to the interval 1.9–11.8 $Å^{-1}$ for the PZ due to a low signal-to-noise ratio at $k>12$ $Å^{-1}$, whereas this parameter for PZT allowed using a wider k range for the Fourier transformation: 1.9–14.4 $Å^{-1}$. The spectra were fitted in the R range 0.9–1.9 Å in both cases. The best results were obtained for the eight- and 12-site models. They are presented in Table II in comparison with the values obtained for the one-site model.

It is necessary to note that within both the eight- and 12-site models we considered that all the Zr atom sites are situated on the surface of the central sphere of small radius r_0 according to the PEFS data. We calculated also the first-shell PRDF in each case and determined from these functions the average Zr–O distance R_0 and its variance Σ^2, which are also presented in Table II. All PRDFs were considered to be a simple superposition of Gaussian functions with the parameters summarized in the same table. The absolute values of the Fourier transform and the full PRDF calculated for PZ and PZT for different models are shown in Figs. 7 and 8.

As one can see, the PRDF obtained for PZ within the one-site model is close to those obtained within the eight- and 12-site models, and the R factors for all the models are almost the same. Thus, the anharmonicity in the cubic phase of the PZ crystal is relatively small. At the same time the $R\nu$ factor, which takes into account the different number of varying parameters, is slightly better for the eight-site model. $R\nu$ is related to the R factor, i.e., the latter is divided by the number of degrees of freedom ν

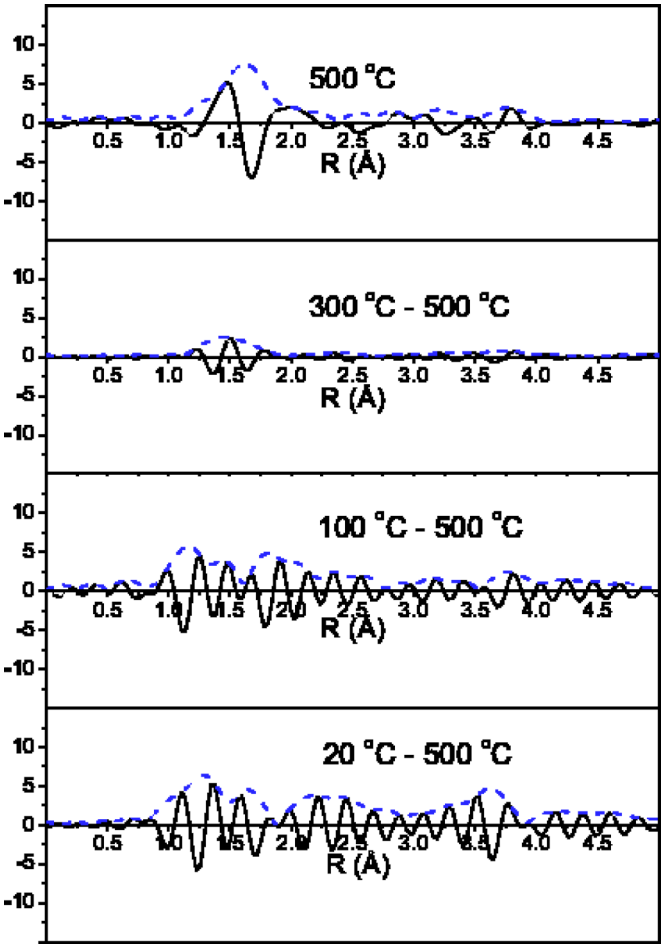

FIG. 9. (Color online) Absolute values [dashed (blue) lines] and real parts [solid (black) lines] of the k^3 weighted FT of the Zr EXAFS signal measured at 500 °C (on the top) and the differential FT for $PbZrO_3$. The temperatures are indicated in the figure.

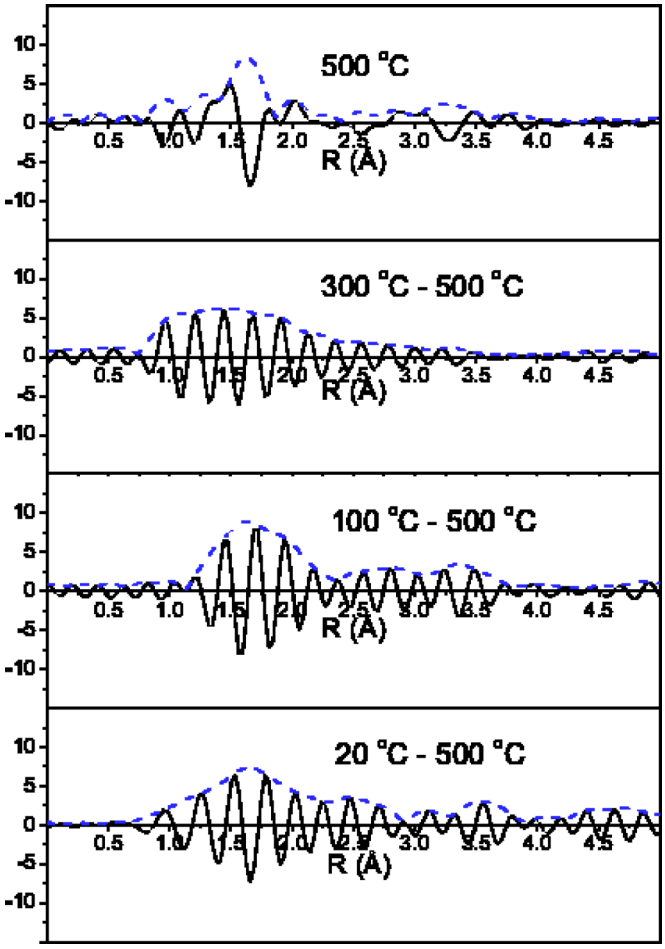

FIG. 10. (Color online) Absolute values [dashed (blue) lines] and real parts [solid (black) lines] of the k^3 weighted FT of the Zr EXAFS signal measured at 500 °C (on the top) and the differential FT for $PbZr_{0.515}Ti_{0.485}O_3$. The temperatures are indicated in the figure.

$$\nu = \left(\frac{2\Delta k \Delta R}{\pi} + 2 \right) - N_{var}, \tag{2}$$

where Δk and ΔR are the fitting ranges in the k and R spaces, and N_{var} is the number of variables in the fit. In the considered case the $R\nu$ factor is useful for clear comparison of the results of fitting because we employ different numbers of varying parameters for the 12-site and the one- and eight-site models.

In the case of PZT the one-site model provides essentially worse R and $R\nu$ factors than the eight- and 12-site models. In addition, the PRDFs, obtained for the last two models are close to each other and are dramatically asymmetric. Hence, the anharmonicity in the cubic phase of the $PbZr_{0.515}Ti_{0.485}O_3$ solid solution is essentially greater than in the cubic phase of PZ and one can resume that the Ti atoms essentially influence the local atomic structure of the ZrO_6 octahedrons in PZT, although the Zr–O average distances are the same for PZ and PZT.

It is worth noting that the calculations for the uniform models provide worse fitting results (the calculated R factor is greater 3% for PZ and PZT crystals) and for the six-site model nonphysical values of the Debye-Waller factor were obtained. Hence, the distribution of the Zr atom on the surface of the central sphere is not uniform even in the cubic phase. The Zr atom occupies several positions on this surface and the number of such positions is not equal to 6.

Taking into account literature data[9,10] and more reliable σ^2 values obtained in the case of the eight-site model, we guess that such local atomic structure is preferable for both PZ and PZT in the cubic phase. If this model (as well as the 12-site model) was appropriate at lower temperatures then the EXAFS signal for the first coordination shell would not change strongly when the temperature decreases as it does in the case of BZ. The Fourier transforms of the difference-EXAFS functions for PZ and PZT are shown in Figs. 9 and 10, respectively. As it follows from Fig. 9, the first-shell signal really changes weakly for PZ in the cubic phase (T =300 °C). On the contrary there is strong temperature dependence below the phase transition points (230 °C for PZ and 360 °C for PZT). This means that either the eight- or 12-site model is not valid for the lower-temperature phases of PZ and PZT and the phase transitions in these crystals cannot be described within the simple order-disorder model.

IV. CONCLUSIONS

The local atomic structure of the perovskite-type zirconates $BaZrO_3$, $PbZrO_3$, and $PbZr_{0.515}Ti_{0.485}O_3$ is studied by Zr *K* spectrum EXAFS and preedge structure analysis in a wide temperature interval. The results obtained in the present paper and previous results for the titanates and niobates reveal that the PEFS intensity is almost temperature independent in the case of powder samples for perovskites suffering structural phase transitions whereas this intensity increases at higher temperatures for perovskites that do not suffer phase transitions. Since the PEFS intensity is determined by the mean square displacement of the *B* atom (B=Zr, Ti, Nb) from the center of the BO_6 octahedron, the temperature independence of PEFS for the perovskites suffering structural phase transitions is assumed to be evidence for the spherical model of the local atomic structure of these crystals. According to this model the *B* atoms at all temperatures are situated on the surface of a sphere of small radius (central sphere) whose center coincides with the immediate center of the BO_6 octahedron at each moment. The spherical model does not presume existence of particular sites for the *B* atoms on this surface, which are the same at all the temperatures, and according to this model the distribution of the *B* atoms on the central sphere surface can depend on the temperature. The results of EXAFS analysis performed for PZ and PZT are in agreement with results of the spherical model. The best results in the cubic phase at 500 °C are obtained for the eight-site model. On the contrary, the differential EXAFS analysis demonstrates that the eight-site model is not appropriate in the case of the lower-symmetry phases of PZ and PZT. Hence, neither displacive nor order-disorder models are sufficient for the description of the phase transitions in the zirconates studied.

The EXAFS and PEFS results reveal strong anharmonicity of the crystal lattice dynamics for PZT whereas it is relatively small for PZ in the cubic phase. The dramatic difference between the local atomic structures of the ZrO_6 octahedrons for PZT and PZ demonstrates a strong influence of the Ti atoms on this structure. On the contrary the crystal lattice dynamics is harmonic for BZ crystals in a wide temperature range.

ACKNOWLEDGMENTS

We are grateful to V. P. Sakhnenko for helpful discussions, L. A. Resnichenko for the sample preparation, J.-L. Hazemann for the help in organization of the experiment, and V. Dmitriev for providing the heater. The studies were supported by the Russian Ministry of Science and Education Grant No. R662. E.N. acknowledges partial support from the French Government (CNOUS).

[1] D. E. Cox, B. Noheda, G. Shirane, Y. Uesu, K. Fujishiro, and Y. Yamada, Appl. Phys. Lett. **79**, 400 (2001).
[2] J. Harada, J. D. Axe, and G. Shirane, Phys. Rev. B **4**, 155 (1971).
[3] R. Comes, M. Lambert, and A. Guinier, Solid State Commun. **6**, 715–719 (1968).
[4] L. Godefroy, A. Derouiche, and A. Benzagouta, Ferroelectrics **54**, 13 (1984).
[5] N. Sicron, Y. Yacoby, E. A. Stern, and F. Dogan, J. Phys. IV **7**, C2-1047 (1997).
[6] N. de Mathan, E. Prouzet, E. Husson, and H. Dexpert, J. Phys.: Condens. Matter **5**, 1261 (1993).
[7] V. A. Shuvaeva, K. Yanagi, K. Yagi, K. Sakaue, and H. Terauchi, Solid State Commun. **106**, 335 (1998).
[8] V. A. Shuvaeva, K. Yanagi, K. Yagi, K. Sakaue, and H. Terauchi, J. Synchrotron Radiat. **6**, 367 (1999).
[9] M. I. Marques, Phys. Rev. B **71**, 174116 (2005).
[10] B. Zalar, V. V. Laguta, and R. Blinc, Phys. Rev. Lett. **90**, 037601 (2003).
[11] O. Proux, X. Biquard, E. Lahera, J.-J. Menthonnex, A. Prat, O. Ulrich, Y. Soldo, P. Trévisson, G. Kapoujvan, G. Perroux, P. Taunier, D. Grand, P. Jeantet, M. Deleglise, J.-P. Roux, and J.-L. Hazemann, Phys. Scr. **115**, 970 (2005).
[12] E. Sawaguchi, G. Shirane, and Y. Takagi, J. Phys. Soc. Jpn. **6**, 333 (1951).
[13] G. Shirane, E. Sawaguchi, and Y. Takagi, Phys. Rev. **84**, 476 (1951).
[14] P. E. Petit, F. Guyot, and F. Farges, J. Phys. IV **7**, C2-1065 (1997).
[15] R. V. Vedrinskii, V. L. Kraizman, A. A. Novakovich, Ph. V. Demekhin, and S. V. Urazhdin, J. Phys.: Condens. Matter **10**, 9561 (1998).
[16] B. Ravel and E. A. Stern, J. Phys. IV **7**, C2-1223 (1997).
[17] B. Ravel, E. A. Stern, and Y. Yacoby, Jpn. J. Appl. Phys., Part 1 **32**, 782 (1993).
[18] B. Ravel and E. A. Stern, Physica B **208/209**, 316 (1995).
[19] V. A. Shuvaeva, Y. Azuma, K. Yagi, K. Sakaue, and H. Terauchi, J. Synchrotron Radiat. **8**, 833 (2001).
[20] J. Kokubun, K. Ishida, D. Cabaret, F. Mauri, R. V. Vedrinskii, V. L. Kraizman, A. A. Novakovich, E. V. Krivitskii, and V. E. Dmitrienko, Phys. Rev. B **69**, 245103 (2004).
[21] M. Newville, J. Synchrotron Radiat. **8**, 322 (1999); http://cars9.uchicago. edu/ifeffit/
[22] Computer code IFEFFIT, Chap. 5, formula (5.7), http:/cars9.uchicago.edu/~newville/feffit/feffit. ps
[23] A. L. Ankudinov and J. J. Rehr, Phys. Rev. B **56**, R1712 (1997).